Magnetic and mechanical properties of additively manufactured Alx(CoFeNi) complex concentrated alloys

Varun Chaudhary, Mohan Sai Kiran Nartu, Sriswaroop Dasari, Sai Sree Meenakshi Varahabhatla, Abhishek Sharma, Madhavan Radhakrishnan, Srinivas Aditya Mantri, Stéphane Gorsse, Narendra Dahotre, Raju V. Ramanujan, et al.

Magnetic and Mechanical Properties of Additively Manufactured Al_x(CoFeNi) Complex Concentrated Alloys

V. Chaudhary[a], M.S.K.K.Y. Nartu[b,c], S. Dasari[b], S.M. Varahabhatla[b,c], A. Sharma[b], M. Radhakrishnan[b,c], S.A. Mantri[b,c], S. Gorsse[d], N.B. Dahotre[b,c], R. V. Ramanujan[a] and R. Banerjee[b,c*]

[a]School of Materials Science and Engineering, Nanyang Technological University, 639798, Singapore

[b]Department of Materials Science and Engineering, University of North Texas, Denton, TX, 76207, USA

[c]Center for Agile and Adaptive Manufacturing (CAAAM), University of North Texas, Denton, TX, 76207, USA

[c]CNRS, Univ. Bordeaux, Bordeaux INP, ICMCB, UMR 5026, 33600 Pessac, France

*Corresponding author: Raj.Banerjee@unt.edu

Abstract

Varying the Al content, strongly influences the microstructure, magnetic and microhardness of additively manufactured Al_x(CoFeNi) (x = 0, 10, 30) complex concentrated alloys (CCA). Compared to the single FCC phase of CoFeNi, the hierarchical FCC/$L1_2$+BCC/B2 heterostructure of heat treated Al_{10}(CoFeNi) CCA displayed substantially improved saturation magnetization, Curie temperature and microhardness. However, there was no significant change in the properties of heat treated CoFeNi and Al_{30}(CoFeNi) CCA. These findings can be rationalized *via* thermodynamic modelling of the phase stability. We have demonstrated the feasibility of exploiting additive manufacturing for rapidly screening and developing novel high-performance alloys for next generation rotating electrical machines.

Keywords: Complex concentrated alloys; additive manufacturing; microstructure; magnetic properties

The development of novel magnetic materials has gained high interest in recent years, especially due to an urgent increase in demand for superior rotating electrical machines operating at high frequency, large torque and elevated service temperatures [1-4]. Most commercial magnetic alloys are based on one or two principal elements alloyed with other minor elements and exhibit low efficiency for next generation high stress, elevated temperature, and large rotating frequency electrical machine applications. Such applications require both mechanical as well as magnetic properties.

There is significant interest in exploring such novel materials using the strategy of complex concentrated alloys (CCA) having multiple principal elements in high concentration[2, 4-8]. A range of CCA have been processed using different techniques and some of them exhibited very interesting magnetic and mechanical properties. However, only a tiny fraction of the possible compositions of CCA has been explored. Tuning the length scale of the complex multiphase microstructures of selected CCA by thermal treatment can result in an optimum set of mechanical and functional properties. Therefore, further research must be performed to discover a novel CCA with a promising multi-property set.

Direct energy deposition (DED), an additive manufacturing (AM) technique, is an emerging method to rapidly explore multiple compositions through accelerated methodologies [9-11]. It can also provide near net shape components, which are challenging to build using conventional techniques, such as casting. DED-AM has been used for printing several types of magnetic materials including, Ni-Fe-V, Fe-Ni-Mo, Co-xFe, Ni-xFe, Fe-Co-Ni, $Al_xCoCrFeNi$, $Al_xCrCuFeNi_2$, etc[4, 9, 12-14].

Conventional approaches of finding a promising material typically involve synthesis and characterization of a few compositions, are expensive, inefficient and time consuming. Instead, we used a thermodynamics-guided approach to reduce the experimental load to identifying promising materials. The primary objective of this study is to rapidly investigate the change in microstructural, magnetic and mechanical properties with Al content in AM processed $Al_x(CoFeNi)$ CCA, thus identifying promising compositions. Al alloying content in $Al_x(CoFeNi)$ (x = 0, 10, 30) was chosen such that three major phase fields in the pseudo-binary isopleth can be explored. High temperature magnetometry, *in-situ* high temperature X-ray diffraction (XRD), Transmission Electron Microscopy (TEM) were performed to determine the magnetic and structural properties at high temperatures.

Al_x(FeCoNi) CCA were printed by an Optomec LENS (Laser Engineering Net Shaping) 750 system using Fe, Co, Ni and Al powders (purity >99.9%), with sizes ranging from 50 to 150 μm. CCA of desired compositions were roller-mixed prior to the deposition. A 1500 W Nd: YAG laser producing near- infrared radiation at a wavelength of 1.064 μm was used to deposit the CCA. The processing parameters were: 300 W laser power; 0.5 mm diameter laser beam on the sample surface; 12.7 mm/s laser scan speed; 0.254 mm vertical layer spacing; 0.381 mm hatch width with 90° rotation in the hatch direction between layers. These combinations of laser parameters provided an input energy fluence of 47.24 J/mm^2. The input energy fluence/energy density was calculated using the expression E = P/V × D, where P is the laser power, V is the scan speed, and D is the laser beam diameter. The oxygen level in the glove box was maintained below 10 ppm to fabricate samples with dimensions of 25.4 mm × 25.4 mm ×25.4 mm. The deposited build was then separated from the steel substrate and subsequently sliced for microstructural and magnetic property measurements using a KENT USA (WSI-200) electric discharge machine (EDM).

The phase constitution was examined by X-ray diffraction (XRD) in a Bruker 8D Advance diffractometer (room temperature) and Bruker 8D Discover diffractometer (for *in-situ* high temperature measurements), using CuKα (1.54 Å) radiation. TOPAS Software was used for Rietveld refinement of the XRD data. Room temperature and high temperature magnetic properties were measured using a physical property measurement system (PPMS) equipped with a vibrating sample magnetometer (VSM). The sweep rate for magnetization versus temperature measurements in the cases of both heating and cooling was fixed at 3 K/min. Imaging and Electron backscatter diffraction (EBSD) analysis was performed in an FEI-Quanta Nova-Nano SEM 230. OIM™ software was used to produce the Inverse Pole Figure (IPF) maps and the Phase maps from the EBSD scans. TEM foils were prepared inside an FEI Nova 200 Nanolab dual-beam Focused ion beam (FIB/SEM) and were characterized using a FEI Tecnai G2 F20 ST S/TEM, a transmission electron microscope (TEM operating at 200 kV) outfitted with a (scanning transmission electron microscopy–energy dispersive spectroscopy) STEM-EDS detector.

Figure 1 (a) shows a pseudo-binary isopleth for the Al_x(CoFeNi) alloy system, with changing Al content, calculated using the TCHEA4 database in Thermocalc. Three compositions of

Al_x(CoFeNi) with x = 0, 10 and 30 were chosen based on the different phase fields they exhibit. The isopleth predicts a single-phase FCC for x = 0 and x = 10, and B2 for x = 30, at a temperature of 1300 °C. With decreasing temperature, there is a substantial change in the phase stability, especially for x = 10. The room temperature XRD data of CoFeNi (Al-0) and Al_{10}(CoFeNi) (Al-10) exhibited a single-phase FCC phase, while Al_{30}(CoFeNi) (Al-30) was a single B2 phase (Figure 1b). The rapid cooling rate (10^3-10^5 °C/sec) in direct energy deposition processes leads to the high temperature phase quenched in to room temperatures[15]. The change in lattice parameters with increasing Al content in Al_x(CoFeNi) is shown in supplementary Figure S1.

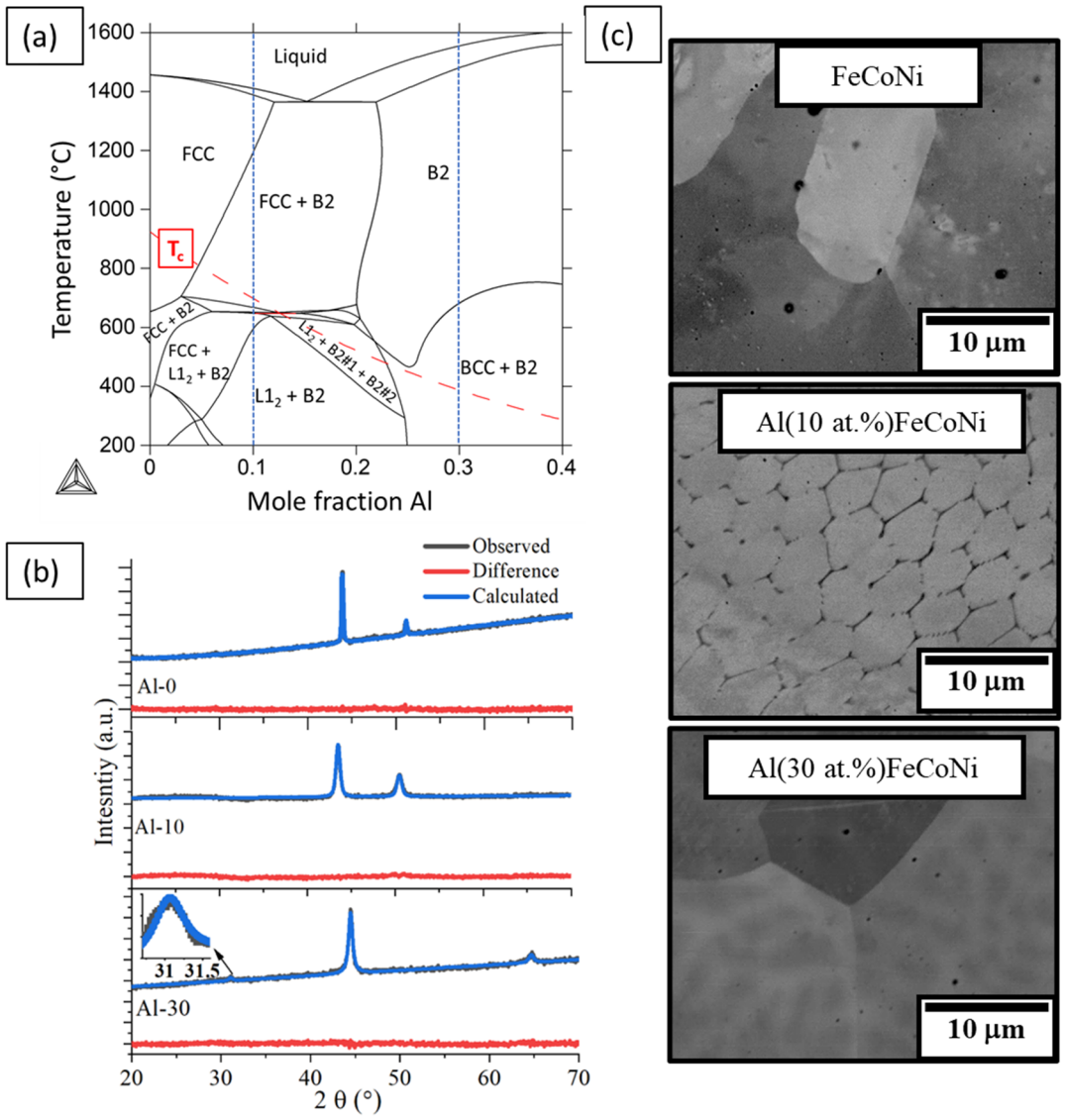

Figure 1. (a) Psuedo-binary isopleth for varying Al in ternary CoFeNi system (b) Rietveld refinement of the X-ray diffraction patterns and (c) SEM backscatter images of Al_x(CoFeNi) CCA.

The backscattered electron images of all three compositions are shown in Figure 1c. CoFeNi and Al_{30}(CoFeNi) exhibited a single-phase FCC and B2 microstructures, respectively. Al_{10}(CoFeNi) also exhibited an FCC matrix with a significant fraction of cellular boundaries arising from solidification.

Figure 2 (a) shows the field dependence of magnetization at room temperature for as deposited Al-0, Al-10 and Al-30 alloys. The saturation magnetization (M_s) decreased from 160 to 61.1 emu/g with increasing Al content from 0 to 30 in Al_x(CoFeNi) CCA. Such a decrease in M_s with increasing Al content can be rationalized by considering the magnetic behaviour of the elements present in Al_x(CoFeNi) CCA. The paramagnetic element (Al) replaced the ferromagnetic elements (Co, Fe, Ni), reducing the effective ferromagnetic moment and therefore M_s.

The Curie temperature is another important performance metric especially for high temperature applications. Figure 2(b) shows the temperature dependence of the magnetic behaviour (M vs. T or M-T) from room temperature to 725 °C in both heating and cooling modes at an applied magnetic field of 100 Oe. All three graphs of M vs. T did not follow the same path while heating and cooling. The most significant difference is in the case of Al-10, there is a steep decrease in the M value around 475°C- 500°C due to the ferromagnetic to paramagnetic transition (T_c) of the FCC matrix. A re-entrant magnetic moment upon heating which begins at ~ 500 °C, goes to a maximum at ~ 625 °C can be clearly observed. This re-entrant magnetization in Al-10 possibly indicates the decomposition of the FCC matrix due to heating. A rationalization of this anomalous change during the M-T cycle is discussed in later sections of this paper.

As printed samples exhibited a H_c of 10.9 Oe, 4.0 Oe and 14 Oe, M_s of 160 emu/g, 125.7 emu/g and 61.1 emu/g, T_c of >725 °C, 475°C and 397 °C for x =0, 10 and 30 in Al_x(CoFeNi) CCA, respectively. The variations in M_s, H_c and T_c with the alloy composition for as deposited and after the M-T heating/cooling cycle are plotted in figure 2 (d, e, and f). Interestingly, the most significant change in all these properties is observed for Al-10. M_s improved from 125.7 to 139.5 emu/g, H_c increased from 4 to 197.3 Oe, and T_c changed from 475°C to 627 °C.

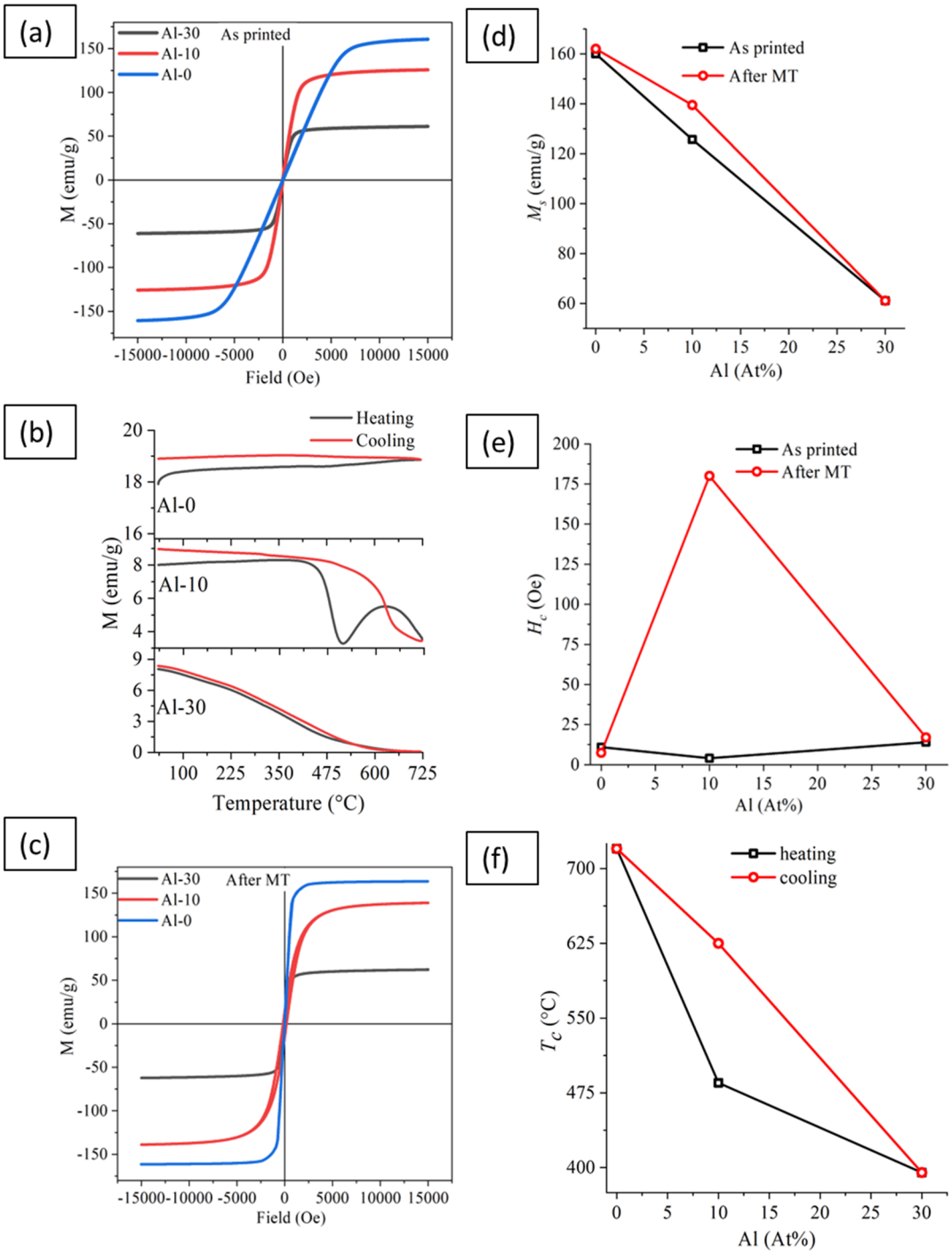

Figure 2. Magnetic properties of Al_x(CoFeNi) CCA at room temperature and elevated temperatures (a) Magnetization (M) as a function of applied magnetic field at room temperature (b) Magnetization versus temperature for heating and cooling at an applied field of 100 Oe. (c) M-H loops after M-T measurement shown in "b". (d) saturation magnetization (M_s), (e) coercivity (H_c) and (f) Curie temperature (T_c) with changing Al content in Al_x(CoFeNi) CCA for as printed and after MT samples.

Figure 3 represents the microhardness plot for varying compositions in Al_x(CoFeNi) CCA for both as printed and after MT samples. For as printed samples, there is a clear trend of increasing Vickers microhardness with higher Al content in CoFeNi. Such a rise in microhardness with increasing Al content has been reported in other multicomponent systems, e.g., AlxCrCuFeNi2[16], AlxCoCrFeNi[17, 18], primarily due to the change in microstructure from FCC to BCC/B2 as well as due to solid solution strengthening arising from multiple principle elements. After the M-T cycle, there is almost no change in microhardness values for Al-0 and Al-30. However, the heat-treated Al-10 sample exhibited ~3 times increase in hardness compared to the hardness for the as deposited Al-10 sample. The microhardness of 577 HV for heat treated Al_{10}(CoFeNi) CCA is higher than those of Al_xCrCuFeNi2[16] and Al_xCoCrFeNi[17, 18] CCA systems, irrespective of the Al content and processing route. Interestingly, the hardness value of this additively manufactured Al_{10}(CoFeNi) CCA is higher than the hardness for a nearly identical composition $Al_{0.3}$CoFeNi processed by conventional casting and superior to famous soft magnetic materials, e.g., permalloy ($Fe_{15}Ni_{80}Mo_5$), permendur ($Fe_{49}Co_{49}V_2$), etc[19].

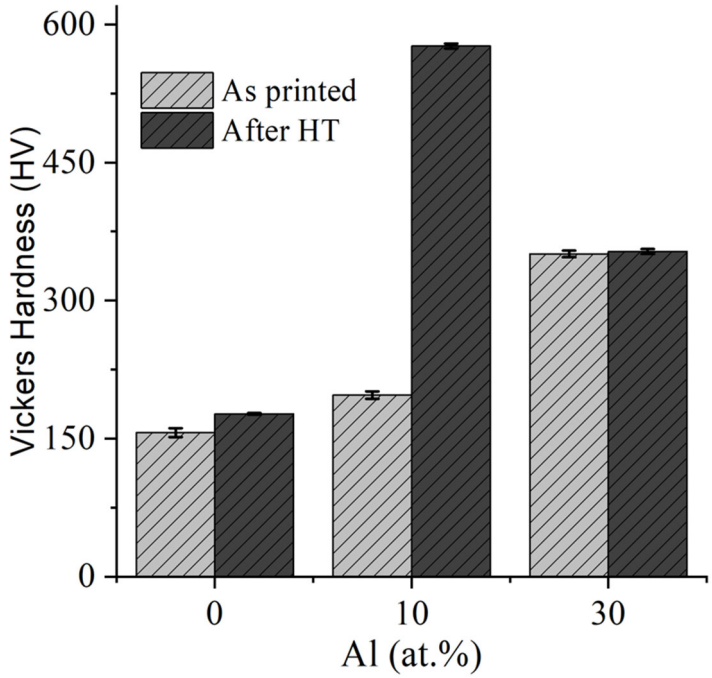

Figure. 3 Variation in microhardness of as printed and after HT with changing the Al content in Al_x(CoFeNi) CCA

To understand these drastic changes in magnetic properties and microhardness values, detailed microstructural characterization was performed on the Al-10 sample in the heat-treated

condition. The SEM backscatter image (in Fig 4(a)) of the Al-10 condition clearly showed lamellar features, resembling pearlite in steels[20] that developed during the heating/cooling cycle of the M-T analysis. A similar lamellar microstructure has been previously reported by Dasari *et al.* in conventionally fabricated and thermo-mechanically processed Al-(9 at%)CoFeNi[21]. On the other hand, such lamellar features are not observed in the other two compositions, i.e., Al-0 and Al-30 conditions that were subjected to similar heating/cooling cycles during the M-T run.

To understand the evolution of the secondary lamellar features, *in-situ* high temperature XRD was performed on the as printed Al-10 condition at different temperatures (27 °C, 500 °C, 600 °C and 725°C) during heating and cooling, the resultant plots are shown in figure 4(b). The maximum temperature of 725 °C is the temperature limit of the instrument. At room temperature, the Al-10 condition is found to consist of a face centered cubic (FCC) phase (f_{FCC}=100%). As the temperature increased to 500 °C, the formation of a BCC phase was observed. The diffraction peak intensity of BCC phase increases with higher temperature up to 725 °C and remained constant during cooling to room temperature. However, a simulated pseudo-binary isopleth using Thermocalc predicts a three-phase field, FCC+B2+$L1_2$ for this alloy composition between 500°C and 600°C (refer to Fig. 1(a)). Since the (110) reflections observed in the XRD pattern (Fig. 4(b)) are allowed for both BCC and B2 phases, it is difficult to distinguish between them using a conventional XRD analysis. The change in phase fraction with increasing temperature is plotted in figure 4(c). Nearly 70% of the FCC matrix decomposed/transformed to the BCC/B2 phases.

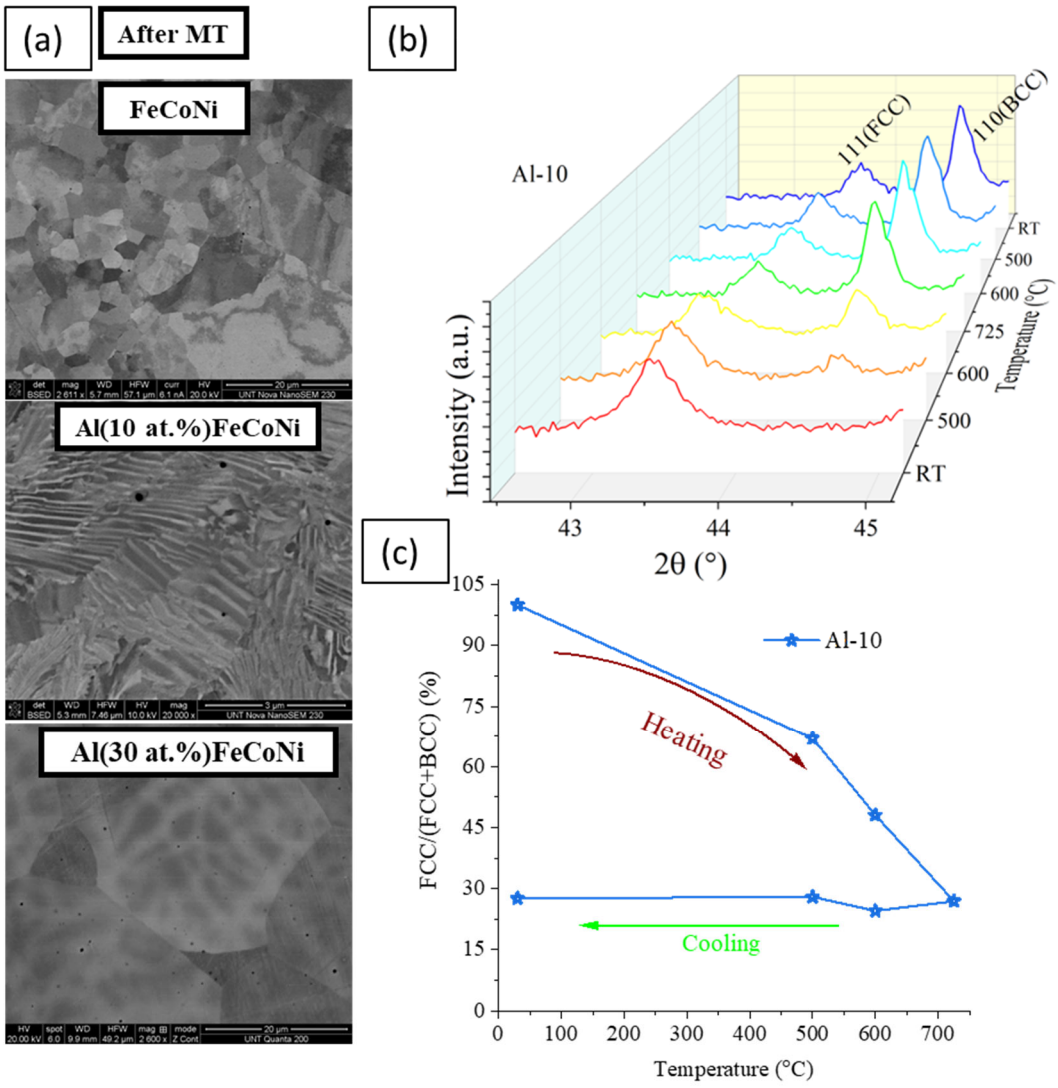

Figure 4. (a) Backscattered electron images of Al_x(CoFeNi) CCAafter MT measurements. (b) The *in-situ* high temperature XRD results for Al_{10}(CoFeNi) CCA in the range from room temperature to 725 °C for both heating and cooling modes. (c) Variation in phase fraction as a function of temperature measured over heating and cooling cycles.

The backscattered SEM images along with Phase and IPF maps obtained from the EBSD scans performed on the Al-10 condition (post MT) are provided in Supplementary Figure S2. The phase map identifies the untransformed regions as FCC and the transformed regions, i.e., the lamellar microstructure, as single-phase BCC. The lamellae are too fine (nano-scale) to be resolved by SEM-EBSD. Therefore, TEM analysis was performed to identify the phases present within the nano-lamellar microstructure.

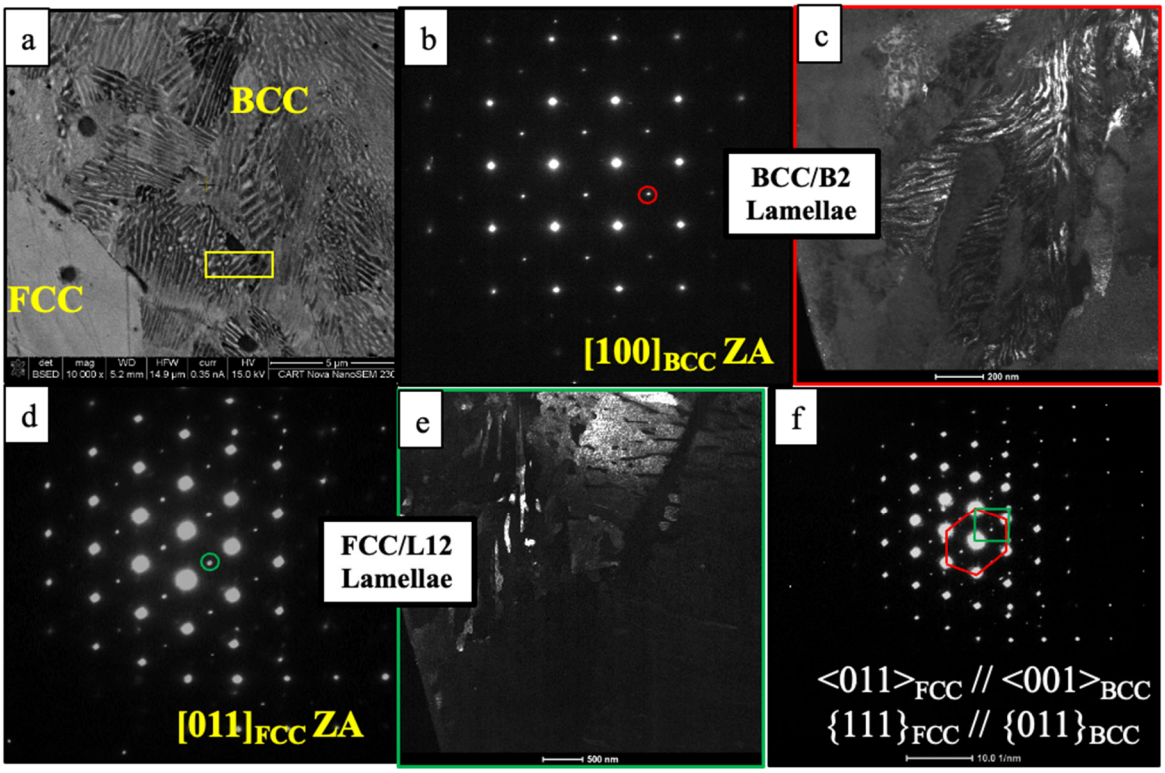

Figure 5. For Al-10 condition samples: (a) SEM backscatter image showing the lamellar microstructure. (b) SAED pattern recorded along the [100] BCC Zone Axis from one of the alternating lamellae shown in Fig. 5(a). (c) DFTEM image, recorded using the {001} B2 superlattice reflection, outlined in red in Fig. 5(b). (d) SAED pattern recorded along the [110] FCC Zone Axis from the other alternating lamellae shown in Fig. 5(a). (e) DFTEM image, recorded using a {001} $L1_2$ superlattice reflection, outlined in green in Fig. 5(d). (f) SAED pattern obtained from the interface of the FCC/BCC lamellae showing the Nishiyama-Wasserman (N-W) orientation relationship between the phases.

The region outlined (in yellow) in Fig. 5(a) represents the area from which the TEM lift-out was prepared. The Selected Area Electron Diffraction (SAED) pattern recorded from one of the alternating lamella, shown in Fig. 5(b), can be indexed as [100] BCC Zone Axis (ZA) exhibiting additional superlattice reflections corresponding to {001} B2. The Dark-field (DF) TEM image, recorded using one of the {001} B2 superlattice reflections (outlined in red in Fig. 5(b)), shown in Fig. 5(c), highlights the B2 regions within the BCC lamellae. Similarly, the SAED pattern shown in Fig. 5(d), recorded from the other alternating lamella can be indexed as the [011] FCC ZA exhibiting {100} type superlattice reflections arising from the ordered

$L1_2$ phase. The corresponding {100} superlattice DFTEM image, presented in Fig. 5(e), highlights the ordered $L1_2$ regions within the FCC lamellae. The SAED pattern obtained from the interface of the FCC/BCC lamellae, showing the Nishiyama-Wasserman orientation relationship between the phases, is presented in Fig. 5(f). Both the DFTEM images in Figs. 5(c) and 5(e) reveal that within each lamella, the BCC and B2 phases and the FCC and $L1_2$ phases are co-continuous in morphology, indicating the possibility of spinodal decomposition coupled with chemical ordering within the lamellae [21].

The improvement in M_s observed before and after MT measurements (from 125.7 to 139.5 emu/g) could be associated with the additional phases formed during the heating cycle of the MT measurements. Atom probe tomography (APT) composition analysis in identical hierarchical FCC/$L1_2$ + BCC/B2 lamellar microstructure in conventionally processed and subsequently annealed Al-(9 at%)FeCoNi CCA revealed a higher percentage of ferromagnetic elements (Fe, Co and Ni) in the BCC phase compared to the FCC, $L1_2$ and B2 phases[21]. Therefore, the higher observed M_s value in the present study could be due to the formation of a signification fraction (70%) of the BCC+B2 phases (from the XRD analysis, Fig. 4(c)) in the Al-10 condition during the heating cycle of the M-T analysis.

Due to the higher T_c of the new B2 and BCC phases forming from the decomposition, the M value increases and reaches a maximum around 625 ℃ (Refer to Fig. 2(b)) during the heating cycle of the M-T analysis. Although the increase in BCC/B2 phase is observed until the maximum temperature of 725 °C, the magnetic moment starts decreasing from 650 °C due to the ferromagnetic to paramagnetic transition of the BCC/B2 phase. M-T measurements upon cooling did not show such a change in magnetic behaviour, and the major transition temperature shifted to higher values by ~ 150 °C. The Curie temperature for the Al-10 alloy measured from the M-T behavior of the cooling cycle was found to be 627 °C. There is no structural transition in this alloy during the cooling cycle, since the decomposition of the FCC phase has already occurred during the heating cycle.

A substantial increase in the H_c can be attributed to the numerous interfaces arising from the FCC/$L1_2$ + BCC/B2 complex hierarchical microstructure. The coercivity of the single-phase FCC in the case of as deposited sample increased ~50 times due to the decomposition into the FCC/L12 + BCC/B2 heterostructure, after M-T measurements. The heterostructure with an

abrupt chemical/phase change in the samples heat treated at 725 °C increases the resistance to the movement of magnetic domain walls, leading to a higher value of coercivity compared to single-phase samples.

Conclusions

Using the example of a $Al_xCoFeNi$ CCA, this study presents a thermodynamics-guided approach for designing novel additively processed CCAs with a good balance of magnetic and mechanical properties. The example presented in this paper investigated the effect of Al content in the $Al_xCoFeNi$ CCA, on the microstructure, magnetic and mechanical properties. These properties were found to change multi-fold due to the composition and microstructural complexity. The addition of non-ferromagnetic Al progressively changes the phase stability from single phase FCC to lamellar FCC/$L1_2$ + BCC/B2 finally to a single B2 phase with attendant reductions in the overall M_s and T_c. These variations in phase stability were accurately predicted via thermodynamic modelling. Equiatomic CoFeNi exhibits a high saturation magnetisation (M_s) and high Curie temperature (T_c) but high coercivity (H_c) and poor mechanical properties. On the other hand, as printed Al_{10}(CoFeNi) CCA exhibit low value of H_c, reasonably good M_s and T_c and a high mechanical hardness. The re-entrant magnetic moment at higher temperatures in Al_{10}(CoFeNi) CCA was associated with a decomposition of the FCC phase to form a lamellar FCC/$L1_2$ + BCC/B2 microstructure, introducing BCC/B2 phases with higher concentrations of ferromagnetic elements. This thermodynamics-guided alloy design through additive manufacturing can be employed in developing materials with balanced magnetic and mechanical properties.

Acknowledgments

This work is supported by AME Programmatic Fund by the Agency for Science, Technology and Research, Singapore under Grant No. A1898b0043. The authors acknowledge the infrastructure and support of Center for Agile & Adaptive and Additive Manufacturing (CAAAM) funded through State of Texas Appropriation #190405-105-805008-220 at the University of North Texas. The authors would also like to acknowledge Materials Research Facility (MRF) for access to advanced characterized techniques.

References

[1] Silveyra JM, Ferrara E, Huber DL, Monson TC. Soft magnetic materials for a sustainable and electrified world. Science. 2018;362:eaao0195.
[2] Chaudhary V, Chaudhary R, Banerjee R, Ramanujan RV. Accelerated and conventional development of magnetic high entropy alloys. Materials Today. 2021;49: 231-52.
[3] Renuka Balakrishna A, James RD. Design of soft magnetic materials. npj Computational Materials. 2022;8:4.
[4] Chaudhary V, Mantri SA, Ramanujan RV, Banerjee R. Additive manufacturing of magnetic materials. Progress in Materials Science. 2020;114:100688.
[5] Lan Q, Kovács A, Caron J, Du H, Song D, Dasari S, Gwalani B, Chaudhary V, Ramanujan RV, Banerjee R, Dunin-Borkowski RE. Highly complex magnetic behavior resulting from hierarchical phase separation in AlCo(Cr)FeNi high-entropy alloys. iScience. 2022;25:104047.
[6] Han L, Rao Z, Souza Filho IR, Maccari F, Wei Y, Wu G, Ahmadian A, Zhou X, Gutfleisch O, Ponge D, Raabe D, Li Z. Ultrastrong and Ductile Soft Magnetic High-Entropy Alloys via Coherent Ordered Nanoprecipitates. Advanced Materials. 2021;33:2102139.
[7] Fu Z, MacDonald BE, Dupuy AD, Wang X, Monson TC, Delaney RE, Pearce CJ, Hu K, Jiang Z, Zhou Y, Schoenung JM, Chen W, Lavernia EJ. Exceptional combination of soft magnetic and mechanical properties in a heterostructured high-entropy composite. Applied Materials Today. 2019;15:590-8.
[8] Han L, Maccari F, Souza Filho IR, Peter NJ, Wei Y, Gault B, Gutfleisch O, Li Z, Raabe D. A mechanically strong and ductile soft magnet with extremely low coercivity. Nature. 2022;608:310-6.
[9] Teh WH, Chaudhary V, Chen S, Lim SH, Wei F, Lee JY, Wang P, Padhy SP, Tan CC, Ramanujan RV. High throughput multi-property evaluation of additively manufactured Co-Fe-Ni materials libraries. Additive Manufacturing. 2022;58:102983.
[10] Ahn D-G. Directed Energy Deposition (DED) Process: State of the Art. International Journal of Precision Engineering and Manufacturing-Green Technology. 2021;8:703-42.
[11] Colorado HA, Velásquez EIG, Monteiro SN. Sustainability of additive manufacturing: the circular economy of materials and environmental perspectives. Journal of Materials Research and Technology. 2020;9:8221-34.
[12] Chaudhary V, Sai Kiran Kumar Yadav NM, Mantri SA, Dasari S, Jagetia A, Ramanujan RV, Banerjee R. Additive manufacturing of functionally graded Co–Fe and Ni–Fe magnetic materials. Journal of Alloys and Compounds. 2020;823:153817.
[13] Nartu MSKKY, Jagetia A, Chaudhary V, Mantri SA, Ivanov E, Dahotre NB, Ramanujan RV, Banerjee R. Magnetic and mechanical properties of an additively manufactured equiatomic CoFeNi complex concentrated alloy. Scripta Materialia. 2020;187:30-6.
[14] Mikler CV, Chaudhary V, Borkar T, Soni V, Jaeger D, Chen X, Contieri R, Ramanujan RV, Banerjee R. Laser Additive Manufacturing of Magnetic Materials. JOM. 2017;69:532-43.
[15] Gibson I, Rosen D, Stucker B. Directed energy deposition processes. Additive manufacturing technologies: Springer; 2015. p. 245-68.
[16] Borkar T, Gwalani B, Choudhuri D, Mikler CV, Yannetta CJ, Chen X, Ramanujan RV, Styles MJ, Gibson MA, Banerjee R. A combinatorial assessment of AlxCrCuFeNi2 (0 < x < 1.5) complex concentrated alloys: Microstructure, microhardness, and magnetic properties. Acta Materialia. 2016;116:63-76.
[17] Li M, Gazquez J, Borisevich A, Mishra R, Flores KM. Evaluation of microstructure and mechanical property variations in AlxCoCrFeNi high entropy alloys produced by a high-throughput laser deposition method. Intermetallics. 2018;95:110-8.

[18] Wang W-R, Wang W-L, Wang S-C, Tsai Y-C, Lai C-H, Yeh J-W. Effects of Al addition on the microstructure and mechanical property of AlxCoCrFeNi high-entropy alloys. Intermetallics. 2012;26:44-51.
[19] Dasari S, Chaudhary V, Gwalani B, Jagetia A, Soni V, Gorsse S, Ramanujan RV, Banerjee R. Highly tunable magnetic and mechanical properties in an Al0.3CoFeNi complex concentrated alloy. Materialia. 2020;12:100755.
[20] Houin JP, Simon A, Beck G. Relationship between Structure and Mechanical Properties of Pearlite between 0.2% and 0.8%C. Transactions of the Iron and Steel Institute of Japan. 1981;21:726-31.
[21] Dasari S, Gwalani B, Jagetia A, Soni V, Gorsse S, Banerjee R. Hierarchical Eutectoid Nano-lamellar Decomposition in an Al0.3CoFeNi Complex Concentrated Alloy. Scientific Reports. 2020;10:4836.